JOURNAL OF MATERIALS SCIENCE 31 (1996) 573–579

Liquid phase sintering of bimodal size distributed alumina powder mixtures

S. TARUTA, T. TAKANO*, N. TAKUSAGAWA
Department of Chemistry and Material Engineering, Faculty of Engineering, Shinshu University, 500, Wakasato, Nagano-shi, Nagano 380, Japan

K. OKADA
Department of Inorganic Materials, Faculty of Engineering, Tokyo Institute of Technology, 2-12-1, Ookayama, Meguro-ku Tokyo 152, Japan

N. ŌTSUKA
Department of Materials, Faculty of Science and Engineering, The Nishi Tokyo University, 2525, Yatsusawa, Uenohara-machi, Kitatsuru-gun Yamanashi 409-01, Japan

Fine and coarse alumina powder mixtures (non-additive specimen) and those containing the additive formed liquid phase during firing (additive specimen) were compacted and fired at 1400–1600 °C. Liquid phase sintering proceeded markedly at 1400–1500 °C and additive specimens had much higher relative density than non-additive specimens at 1500 °C. As the liquid phase sintering proceeded, the open pore volume decreased abruptly, but the open pore size changed depending on the packing structure. The open pore size decreased in the specimens where the fine particles formed matrix structure, while it increased in the specimens where the coarse particles formed skeletal structure. At 1600 °C all additive specimens having different mixing ratios of fine and coarse powders had similar microstructure and the same relative density of 97%. However, spherical large pores were formed and remained in all additive specimens even at 1600 °C. The bending strength of those specimens was about 400 MPa.

1. Introduction

Bimodal size distributed powder mixture, which contains two kinds of powders having extremely different particle sizes, enables one to have higher packing density. Such packing is known as the Furnas' packing model [1]. The high packing density of the green compact made from such a powder mixture is advantageous in developing near net shape ceramics and makes low temperature sintering possible. The packing and sintering behaviour of such bimodal size distributed alumina powder mixtures [2–6] have been studied. The results showed that though a green compact having a maximum packing density of 75% was obtained, it was difficult to densify such green compacts at lower temperature owing markedly to grain growth and pore enlargement. Then, zirconia powder, which inhibits grain growth of alumina, was added to the bimodal size distributed alumina powder mixtures [7]. The results showed that the densification was improved by zirconia addition in the compacts containing small amounts of coarse powder, but not in the compacts containing large amounts of coarse powder.

If liquid phase sintering takes place during firing, it is possible to densify the compact at lower temperature in many cases. Particle rearrangement and solution–reprecipitation are known as the mechanisms of liquid phase sintering. Material transfer for solution–reprecipitation involves a route that small particles dissolve into the liquid phase and then the solute reprecipitates on large particles. Such material transfer will be effective on the densification of bimodal size distributed alumina powder mixtures.

In this study, liquid phase sintering of bimodal size distributed alumina powder mixtures was carried out. The powder mixture having the composition of the eutectic point of tridymite–protoenstatite–cordierite, which forms a liquid phase at the lowest temperature of 1355 °C in the SiO_2–Al_2O_3–MgO system [8], was used as the additive to form liquid phase during firing. The effects of the additive on sintering behaviour and the relationship between sintering behaviour and packing structure were discussed. Bending strength was measured for the compacts fired at 1600 °C.

* *Present address*: Research and Development Center, Japan Insulation Co., Ltd, 4064-1, Kitanuma, Nodashinden Hozumi-cho, Motosu-gun, Gifu 501-02, Japan.

0022–2461

2. Experimental procedure

2.1. Alumina powders

Coarse alumina powder with a particle size of > 3 μm in Stokes' diameter, which was classified from a commercial alumina powder (ALM-44, Sumitomo Chemical Co., Japan), and a fine alumina powder (AES-12, Sumitomo Chemical Co., Japan) were used. The average particle sizes of these powders, which were measured by centrifugal particle size analysis, were 4.68 and 0.51 μm, respectively.

2.2. Preparation of additive

Fixed amounts of tetraethyl orthosilicate, magnesium nitrate and aluminium nitrate were dissolved into ethanol, and then an ammonia solution was added to the ethanol solution to make a precipitate. The precipitate was dried, and heated at 800 °C for 1 h and subsequently at 1300 °C for 10 h. The prepared product was a mixture of alumina, cristobalite, enstatite and cordierite, which was analysed by X-ray diffraction (XRD) methods. This product was ground in a ball mill using an alumina pot and balls, and fine particles of < 1 μm in size were classified from the milled powder by elutriation using ethanol as solvent. The classified fine powder was used as the additive, which had an average particle size of 1.01 μm.

2.3. Preparation of green and sintered compacts

The additive, fine and coarse alumina powders were mixed with ethanol in a ball mill using a plastic pot and iron balls coated with plastic. The mixing ratio of the additive was constant at 6.7 vol % (5 wt %), that of the coarse powder was changed at intervals of 10 vol % from 0 to 93.3 vol %, and the rest was the mixing ratio of the fine powder. The powder mixtures were dried, calcined at 600 °C and passed through a 100 mesh sieve. The prepared powder mixtures were compacted by isostatic press at 98 MPa and then fired at 1400–1600 °C for 2 h. The powder mixtures containing no additive were also prepared similarly, but were mixed with a fixed amount of magnesium nitrate which was equivalent to 0.1 wt % MgO.

In this report, the mixing ratio is shown by volume per cent of the coarse alumina powder, V_c. The specimens containing additive and no additive are denoted by additive specimen and non-additive specimen, respectively.

2.4. Measurement and observation

For the green compacts, the bulk density was calculated from the measured weight and volume, and the sintered compact was measured by Archimedes' method using water. The theoretical density of the green compacts was calculated from the theoretical density of alumina and the true density of the additive which was measured by the pycnometer method. The true density of the sintered compact was measured using the ground specimens. The relative density was calculated from these theoretical or true density and from the measured bulk density. Open pore size distributions (average open pore sizes) of the green and the sintered compacts were measured with an Hg porosimeter. Microstructure was observed using scanning electron microscopy (SEM) for the sintered compacts, which were polished and thermally etched at 100–200 °C lower than the firing temperature for 1 h. Crystalline phases of the sintered compacts were analysed by XRD. For the specimens sintered at 1600 °C for 2 h, three point bending strength was measured at room temperature.

3. Results and discussion

3.1. Relative density of green compacts

Relative densities of the green compacts are shown in Fig. 1. The relative densities of both additive and non-additive specimens reached a maximum value at $V_c = 60\%$. However, additive specimens had lower relative density than non-additive specimens at the same mixing ratio. The particle size of the additive was an intermediate value between that of the fine and the coarse alumina powders. That is, the particle size ratio of the coarse powder to the additive and those of the additive to the fine powder were smaller than those of the coarse powder to the fine powder. These particle size ratios largely influence the packing density of the mixtures, and the packing density becomes higher as the particle size ratio increases [9]. Accordingly, the packing of fine and coarse particles in additive specimens must be impeded by the additive particles. These results also indicate that the packing structure of additive specimens were more non-uniform than that of non-additive specimens.

3.2. Densification caused by liquid phase sintering

3.2.1. Relative density

Relative densities of the specimens sintered at 1400–1600 °C for 2 h are shown in Fig. 2. At 1400 °C,

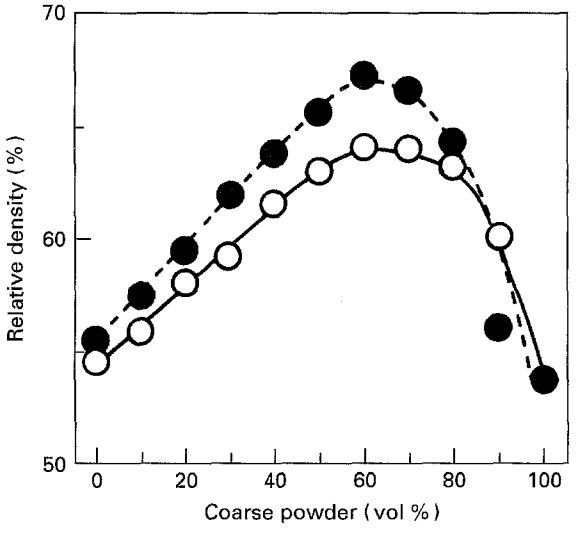

Figure 1 Relative densities of green compacts: (○) additive specimens, (●) non-additive specimens.

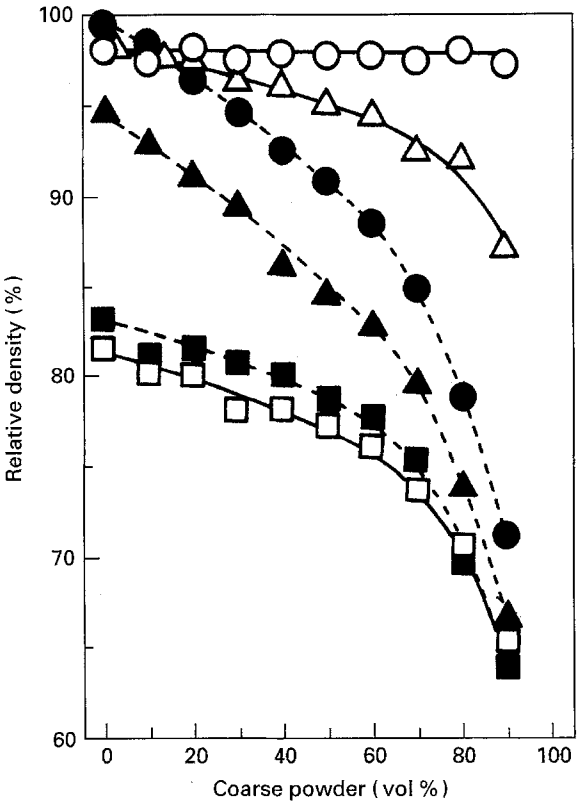

Figure 2 Relative densities of sintered compacts: additive specimens fired at (□) 1400, (△) 1500 and (○) 1600 °C, respectively, and non-additive specimens fired at (■) 1400, (▲) 1500 and (●) 1600 °C, respectively.

additive specimens had lower relative density than non-additive specimens. The amount of liquid phase was so little that liquid phase sintering almost did not influence the densification of additive specimens at 1400 °C. At 1500 °C, additive specimens had much higher relative density than non-additive specimens. These results indicate that liquid phase sintering proceeded markedly at 1500 °C. Moreover, the specimens containing larger amounts of fine powder were densified more than the specimens which contained larger amounts of coarse powder and had higher green density. At 1600 °C, the relative densities of all additive specimens reached about 97%, while non-additive specimens had lower relative density, except for $V_c = 0$–10%. The liquid phase sintering was very effective on the densification of the specimens containing larger amounts of coarse powder. If the packing density of green compacts is enhanced furthermore and particle rearrangement takes place using an additive which forms a liquid phase at lower temperature, densification will be improved.

3.2.2. Average open pore size and open pore volume

Average open pore sizes of the specimens for $V_c = 0$, 30 and 70% are shown in Fig. 3 where G.C. means green compact. Although the green densities of additive specimens were lower than those of non-additive specimens as shown in Fig. 1, the average pore sizes of such additive and non-additive specimens were almost the same. These facts resulted from broader pore size

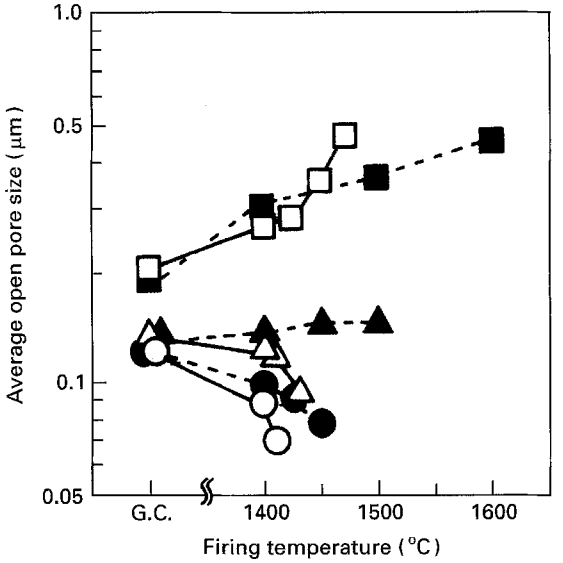

Figure 3 Plots of average open pore size versus firing temperature: additive specimens for V_c = (■) 0, (△) 30 and (○) 70%; and non-additive specimens for V_c = (■) 0, (▲) 30 and (●) 70%.

distributions of additive specimens. With increasing firing temperature, the average open pore size of non-additive specimens for $V_c = 0\%$ decreased, for $V_c = 30\%$ increased slightly and for $V_c = 70\%$ increased abruptly. The increase in pore size is caused by non-uniform sintering as explained in detail in another paper [3]. Comparing such average open pore sizes of non-additive specimens with those of additive specimens, those of additive specimens for $V_c = 0$ and 30% decreased more abruptly, but for $V_c = 70\%$ increased more abruptly above 1400 °C where liquid phase sintering proceeded markedly. Plots of the average open pore size versus the relative density are shown in Fig. 4, in which the relative density was substituted for the firing temperature on the axis of abscissa in Fig. 3. The average open pore sizes of additive specimens for $V_c = 0$ and 30% were smaller, but for $V_c = 70\%$ was almost the same as those of non-additive specimens at the same relative density. Plots of water absorption versus relative density of the sintered compacts are shown in Fig. 5. This figure shows that the open pore volume decreased with increasing relative density, and additive specimens had less open pore volume than non-additive specimens at the same relative density.

The above results indicate that the abrupt decrease in the open pore size of additive specimens for $V_c = 0$ and 30% was caused by the abrupt decrease in the open pore volume owing to rapid densification near the surface of specimens, and that the open pore size of additive and non-additive specimens for $V_c = 70\%$ increased by the same mechanism.

3.3. Crystalline phases

For additive specimens fired at 1400–1600 °C, crystalline phases were determined. Cordierite appeared at 1400 °C, mullite and spinel appeared at 1500 °C, but no crystalline phase was precipitated at 1600 °C. The additive formed not only liquid, but also compounds by solid reaction at 1400 and 1500 °C, and

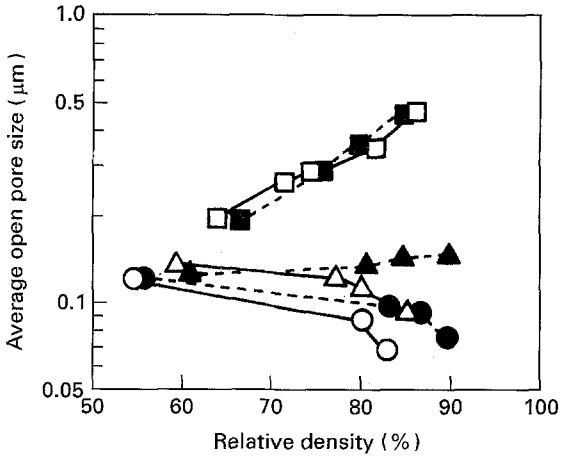

Figure 4 Plots of average open pore size versus relative densities: additive specimens for V_c = (○) 0, (△) 30 and (□) 70%; and non-additive specimens for V_c = (●) 0, (▲) 30 and (■) 70%.

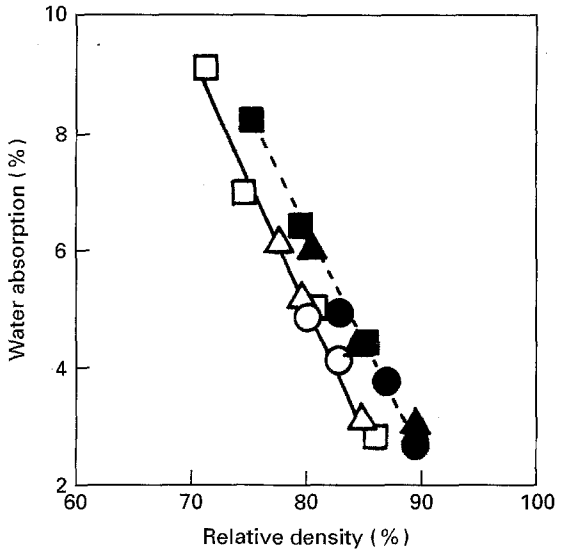

Figure 5 Plots of water absorption versus relative densities: additive specimens for V_c = (○) 0, (△) 30 and (□) 70%; and non-additive specimens for V_c = (●) 0, (▲) 30 and (■) 70%.

then formed liquid completely at 1600 °C. The liquid phase turned into a glass phase during cooling.

3.4. Microstructure

SEM photographs of additive specimens for $V_c = 0$ and 93.3%, which contained no coarse alumina powder and only coarse alumina powder respectively, sintered at 1500 and 1600 °C for 2 h are shown in Fig. 6. At 1500 °C, the densification and the grain growth proceeded much and abnormal grain growth was observed in the specimen for $V_c = 0\%$, while the coarse particles formed skeletal structure and a lot of large pores were observed in the specimen for $V_c = 93.3\%$. These photographs indicate that the sintering mechanism was solution–reprecipitation. That is, fine particles dissolved more into the liquid phase and then the solute precipitated on coarse particles. At 1600 °C, densification and grain growth of the specimens for $V_c = 0$ and 93.3% proceeded further, and these microstructures became almost the same. Small particles

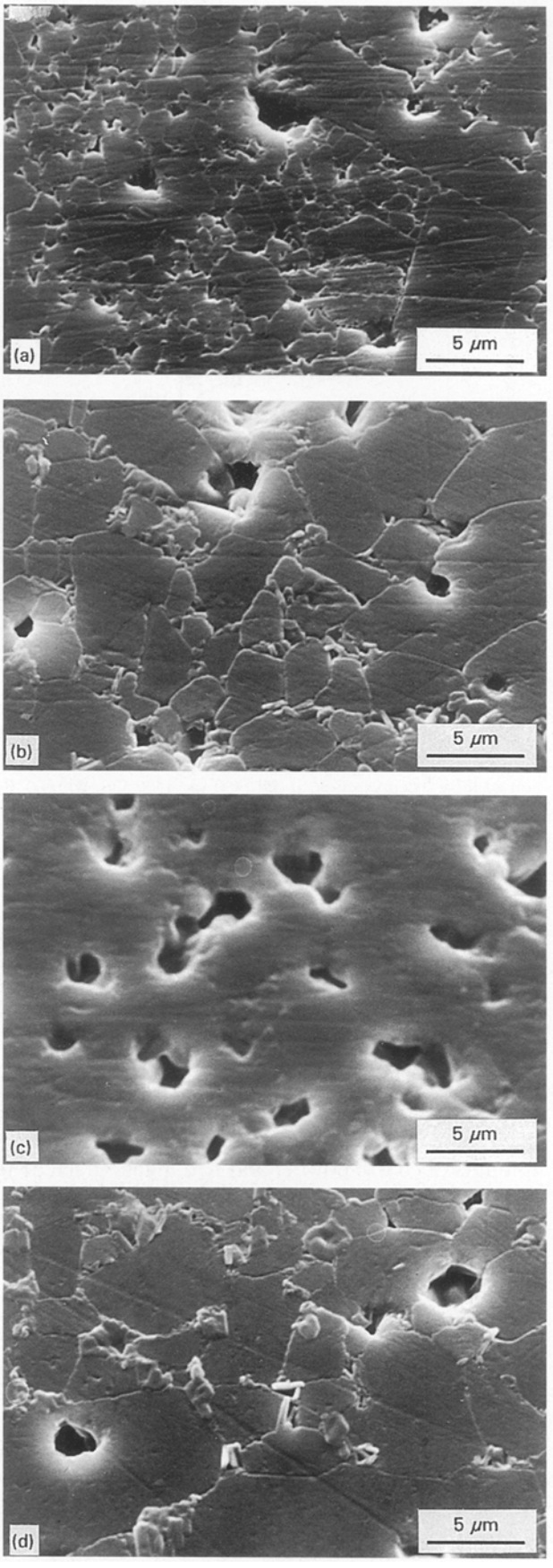

Figure 6 SEM photographs of additive specimens for $V_c = 0\%$ fired (a) at 1500 °C and (b) at 1600 °C, and additive specimens for $V_c = 93.3\%$ fired (c) at 1500 °C and (d) at 1600 °C.

observed in the grain boundary were probably crystalline phases precipitated in the glass phase during thermal etching. Also, spherical large pores of a few micrometer in size were observed in both specimens

for $V_c = 0$ and 93.3%. The formation of such spherical large pores was explained by the following three causes

1. Large particles or agglomerated particles of the additive melted and spread into the capillaries among alumina particles, and then large pores were formed at prior large or agglomerated particles sites [10].
2. The additive particles in the gaps of the skeletal structure of the coarse particles melted, and then large pores were formed in the gaps.
3. As the additive melted, non-uniform sintering took place owing to the non-uniform packing structure [3], and then large pores were formed.

Large pores in the specimens for $V_c = 0$ and 93.3% were formed mainly by points one and two, respectively. The cause of point three was common for $V_c = 0$ and 93.3%.

SEM photographs of additive specimens for $V_c = 30$ and 70% sintered at 1500 and 1600 °C for 2 h are shown in Fig. 7. Comparing the microstructure in Fig. 7 with that in Fig. 6, the microstructure for $V_c = 30$ and 70% resemble that for $V_c = 0$ and 93.3% at 1500 °C, respectively. For all V_c values, differences in the microstructure did not appear at 1600 °C. These microstructures consisted of large grains and spherical pores 2–3 μm in size.

3.5. Sintering process

The above results indicate that although all additive specimens had the same relative density and the same microstructure at 1600 °C, there were two kinds of sintering processes occurring in the additive specimens. One of the sintering processes was observed for $V_c = 0$ and 30%, and the other for $V_c = 70$ and 93.3%. It was thought that these sintering processes varied depending on the packing structure of the green compacts. The sintering process for $V_c = 0$ and 30% is illustrated in Fig. 8a and for $V_c = 70$ and 93.3% in Fig. 8b. The packing structure of the green compacts for $V_c = 0$ and 30% consisted of a matrix of fine particles and coarse particles dispersed in the matrix, and for $V_c = 70$ and 93.3% consisted of a skeletal structure of coarse particles and fine particles packed into the gaps of the skeletal structure. At 1400 °C, the densification of all additive specimens proceeded mainly by solid phase sintering. Above 1400 °C where the additive melted, sintering of each additive specimen proceeded as follows:

1. $V_c = 0$ and 30%: The densification of additive specimens containing larger amounts of fine particles proceeded rapidly at 1400–1500 °C, especially near the surface of the specimen, and the open pores decreased in size and volume. However, spherical large pores formed by points one and two given earlier, and were observed inside the specimen, while crack-like large pores, which were formed in non-additive specimens by separation between fine and coarse particles [3], seemed difficult to form. These facts suggest that solution–reprecipitation not only among the fine particles but also between the fine and the coarse particles took place in additive specimens and also that the

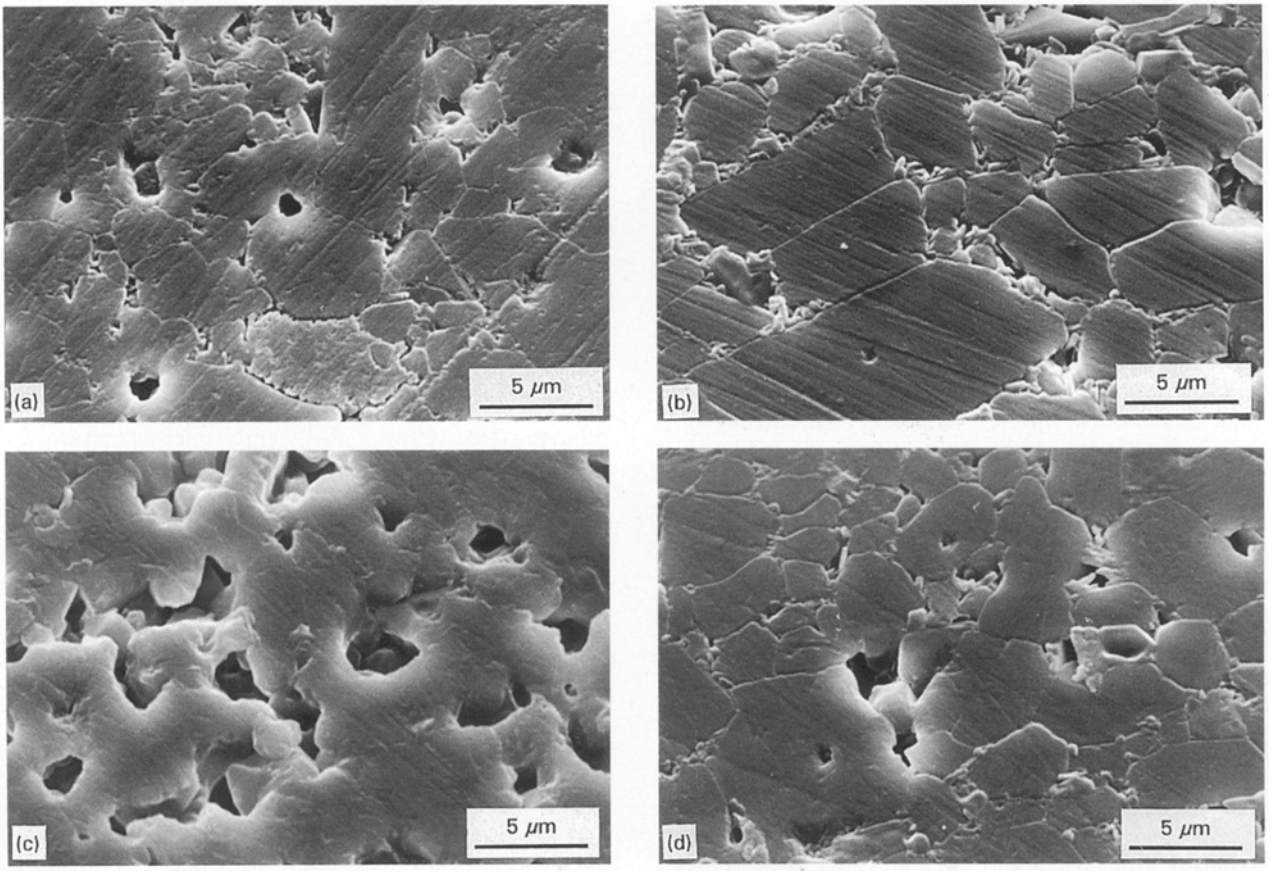

Figure 7 SEM photographs of additive specimens for $V_c = 30\%$ fired (a) at 1500 °C and (b) at 1600 °C, and additive specimens for $V_c = 70\%$ fired (c) at 1500 °C and (d) at 1600 °C.

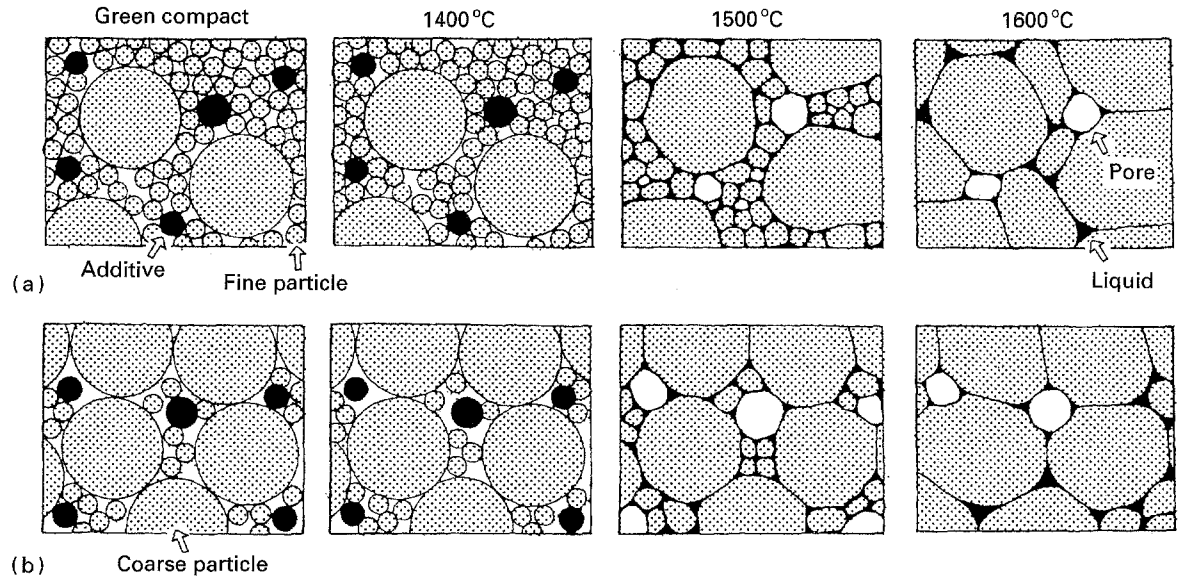

Figure 8 Schematic sintering processes of additive specimens (a) for $V_c = 0$ and 30%, and (b) for $V_c = 70$ and 93.3%.

specimens containing larger amounts of fine powder were densified more because solution–reprecipitation was controlled by an interface reaction in this system [11] and fine particles were more easy to dissolve into the liquid phase. At 1500–1600 °C, densification proceeded further. However, spherical large pores still remained and the density did not reach the theoretical value even at 1600 °C, where grain growth occurred markedly and most of the fine particles disappeared. From these facts, the sintering process at these higher temperatures was considered to be the same as that at 1400–1500 °C. Additive specimens for $V_c = 0$–50% experienced probably the same sintering process, because these specimens had a packing structure similar to that shown in Fig. 8a.

2. $V_c = 70$ and 93.3%: In additive specimens for $V_c = 70$ and 93.3% the coarse particles formed the skeletal structure. Densification among these coarse particles proceeded by liquid phase sintering and the open pore volume decreased abruptly at 1400–1500 °C. However, non-uniform sintering occurred due to the non-uniform packing structure of green compacts [3], and the fine particles packed into the gaps of the skeletal structure sintered each other and localized in the gaps and then larger pores were formed there. That is, the spherical large pores were formed by points two and three given earlier. The open pore size in additive specimens for $V_c = 70\%$ increased abruptly above 1400 °C, as shown in Fig. 3. However, additive and non-additive specimens for $V_c = 70\%$ had the same average open pore size at the same relative density shown in Fig. 4. These facts suggest that sintering proceeded in a similar way in additive and non-additive specimens. That is, densification of these specimens was dominated by densification of the skeletal structure of the coarse particles. With increasing firing temperature, densification of the skeletal structure proceeded and smaller pores disappeared, while larger pores continued to increase. The grain growth of the coarse particles proceeded, but was

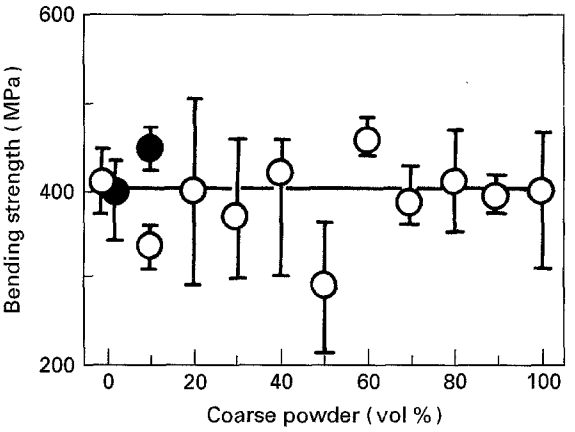

Figure 9 Bending strength of specimens fired at 1600 °C for 2 h: (○) additive specimens, and (●) non-additive specimens.

restricted to a small extent even at 1600 °C because the coarse particles were surrounded by a number of coarse particles which formed the skeletal structure. As a result, even though the coarse particle content was different, all additive specimens had the same relative density and the same microstructure at 1600 °C. Additive specimens for $V_c = 60$–93.3% probably experienced the same sintering process because these specimens had a packing structure similar to that shown in Fig. 8b.

3.6. Bending strength

Bending strengths of additive specimens and a couple of non-additive specimens fired at 1600 °C for 2 h are shown in Fig. 9. The average bending strength of all specimens was about 400 MPa. This result indicates that the bending strength was probably influenced by the fracture origin of large pores existing in all specimens, rather than by the difference in mixing ratio of fine/coarse powder and the sintering process.

4. Conclusions

In this study, the influence of liquid phase on the sintering of bimodal size distributed alumina powder mixtures was discussed. The following conclusions were obtained.

1. The additive formed liquid phase during firing was mixed in alumina powders consisting of different amounts of fine and coarse particles. At 1400–1500 °C, the densification of the powder mixtures proceeded markedly by liquid phase sintering. The densification was faster than that caused by solid phase sintering. Also, the densification of specimens containing larger amount of fine powder was faster than that of specimens containing large amounts of coarse powder. At 1600 °C, densification and the grain growth proceeded further. Consequently all specimens having different mixing ratios had the same relative density of 97% and the same microstructure.

2. As liquid phase sintering proceeded, open pore volume decreased abruptly; however, open pore size changed depending on the packing structure of the green compacts.

3. For $V_c = 0$ and 30%, the packing structure consisted of a matrix of fine particles and coarse particles dispersed in the matrix. The open pore size in the liquid phase sintered compact became smaller than that in the solid phase sintered compact. However, spherical large pores were formed during liquid phase sintering. Such large pores did not disappear completely even at high temperature and the density of the compact did not reach the theoretical value.

4. For $V_c = 70$ and 93.3%, the packing structure consisted of a skeletal structure of coarse particles and fine particles packed into the gaps of the skeletal structure. The open pore size in the liquid phase sintered compact became larger than that in the solid phase sintered compact. However, the open pore size of both the liquid and the solid phase sintered compacts was almost the same as if these compacts had the same relative density.

5. All specimens densified by liquid phase sintering had a bending strength of about 400 MPa at room temperature and the influence of the mixing ratio of the coarse powder on the bending strength was not seen.

References

1. G. L. MESSING and G. Y. ONODA JR, *J. Amer. Ceram. Soc.* **61** (1978) 1.
2. S. TARUTA, K. OKADA and N. ŌTSUKA, *Seramikkusu Ronbunshi* **96** (1988) 146.
3. *Idem, ibid.* **98** (1990) 29.
4. S. TARUTA, K. KITAJIMA, N. TAKUSAGAWA, K. OKADA and N. ŌTSUKA, *ibid.* **99** (1991) 1189.
5. S. TARUTA, K. KITAJIMA, N. TAKUSAGAWA, Y. TAKAGI, K. OKADA and N. ŌTSUKA, *J. Mater. Sci. Lett.* **12** (1993) 424.
6. S. TARUTA, K. KITAJIMA, N. TAKUSAGAWA, K. OKADA and N. ŌTSUKA, *J. Ceram. Soc. Jpn* **101** (1993) 583.
7. S. TARUTA, K. KAWASHIMA, K. KITAJIMA, N. TAKUSAGAWA, K. OKADA and N. ŌTSUKA, *ibid.* **102** (1994) 139.
8. E. M. LEVIN, C. R. ROBBINS and H. F. McMURDIE, "Phase Diagrams for Ceramist" (The American Ceramic Society, Columbus, OH, 1964) p. 246.
9. R. K. McGEARY, *J. Amer. Ceram. Soc.* **44** (1961) 513.
10. R. M. GERMAN, "Liquid Phase Sintering" (Plenum Press, New York, London, 1985) p. 85.
11. O. H. KWON and G. L. MESSING, *J. Amer. Ceram. Soc.* **73** (1990) 275.

Received 6 February
and accepted 17 July 1995